13th IEA Heat Pump Conference
April 26-29, 2021 Jeju, Korea

Residential Split Heat Pump Using Low GWP Refrigerants

Bo Shen*, Moonis Ally

Building Equipment Research Group, Building Technologies Research and Integration Center, Oak Ridge National Lab, TN, USA

Abstract

Conventional refrigerants, e.g. R-410A have high global warming potentials (GWP) > 1800. They are being phased out to protect the environment. The candidates to replace R-410A include R-32, R-452B, R-454B and R-466A for heat pump applications. These candidates are intended for drop-in replacement, i.e. having minimum modifications on existing systems. The paper investigates the low GWP refrigerants drop-in application via system simulations using a well-regarded, hardware-based heat pump model. A baseline heat pump having all fin-and-tube heat exchangers and a two-speed compressor was used. Cross-comparisons were made under rated conditions of ambient temperatures, compressor speeds, indoor air flow rates, respectively for cooling and heating operations. The seasonal performance indices, i.e. SEER and HSPF are presented.

© HPC2020.
Selection and/or peer-review under responsibility of the organizers of the 13th IEA Heat Pump Conference 2020.

Keywords: Heat Pump, Low GWP Refrigerant, System Simulation.

1. Introduction

The earth continues to see a record increase in temperatures and extreme weather conditions that is largely driven by anthropogenic emissions of warming gases such as carbon dioxide and other more potent greenhouse gases such as refrigerants. The cooperation of 188 countries in the 21st Conference of the Parties in Paris 2015 (COP21) resulted in an agreement aimed to achieve universal agreement on climate, with the aim of keeping global warming below 2°C by the end of the century. A global phasedown of hydrofluorocarbons (HFCs) can prevent 0.5°C of warming by 2100.

To replace HCFC and HFC refrigerants in existing air conditioner/heat pump equipment, selections of alternative lower GWP refrigerants are subject to a few key factors. The candidates are expected to have similar volumetric capacity, so that available compressors would provide similar cooling capacity, and equal or higher energy efficiency. In addition, a selected refrigerant should accommodate the same or wider working envelope, i.e. an adequately high refrigerant critical temperature for high ambient operation. Similar or moderately higher compressor discharge temperature levels are also important, to prevent the need to change compressor lubricant and maintain good reliability.

Potential low GWP refrigerants for R-410A used in the study are introduced in Tables 1. The R-410A replacements are mostly blends containing R-32 and an HFO (Hydrofluoroolefins) of R-1234yf, as well as a pure refrigerant of R-32. They have approximately 70% lower GWPs than R-410A. On the other hand, the compositions of R-32 and R-1234yf cause minor flammability and are classified as A2L. It should be noted that R-466A is an A1 refrigerant, i.e. non-flammable. These refrigerant blends have negligible temperature glides. All the alternatives have higher critical temperatures than R-410A, making them more suitable for high condensing temperature operation.

* Corresponding author. Tel.: +1-865-574-5745.
E-mail address: shenb@ornl.gov.

Table 1. Alternative Low GWP Replacements for R-410A

Refrigerant	GWP AR4[a]	GWP AR5[b]	Safety Class	Temperature glide [K]	Critical T [C]
R-410A[c]	2088	1924	A1	0.1	71.34
R-32	675	677	A2L	0.0	78.12
R-452B[d]	698	676	A2L	1.3	79.68
R-454B[e]	466	467	A2L	1.5	77.0
R-466A[f]	733	733	A1	1.5	83.8

a. IPCC 2007.
b. IPCC 2013.
c. R-410A has mass-based compositions of R-32 (0.5)/R-125 (0.5).
d. R-452B has mass-based compositions of R-32 (0.67)/R-125 (0.07)/R-1234yf (0.26).
e. R-454B has mass-based compositions of R-32 (0.689)/R-1234yf (0.311).
f. R-466A has mass-based compositions of R-32 (0.49) / R-125 (0.115) / R-13I (0.395).

2. Refrigerant Properties

The temperature-enthalpy diagram of a refrigerant illustrates two critical properties: the span between the saturated liquid line and saturated vapor line (i.e. latent heat of vaporization per unit mass of refrigerant) and the critical temperature (working range). Volumetric vaporization heat, i.e. latent heat × vapor density at an average saturation temperature of dew point and bubble point, indicates the evaporating capacity per unit volumetric flow rate. Refrigerants with smaller volumetric vaporization heat have reduced cooling capacities at a fixed compressor displacement volume.

Figure 1 illustrates the temperature-enthalpy diagram of R-410A and its alternative refrigerants. All the R-410A alternatives (except R-466A) have wider domes and higher critical temperatures, indicating that they are better refrigerants for high ambient operations. Figure 2 shows the volumetric vaporization heat versus the average saturation temperature. R-32 has noticeably larger vaporization heat than R-410A, and R-466A is slightly larger. R-452B and R-454B have similar vaporization heat, which are slightly lower than R-410A. When approaching to the critical temperature, all the refrigerants' vaporization heat drops.

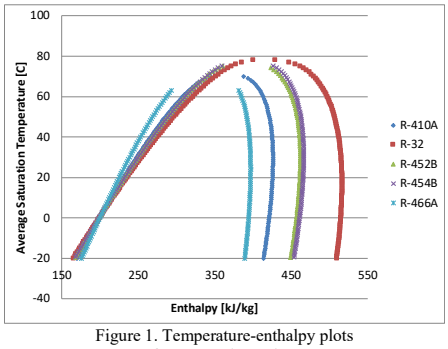

Figure 1. Temperature-enthalpy plots of R-410A alternatives.

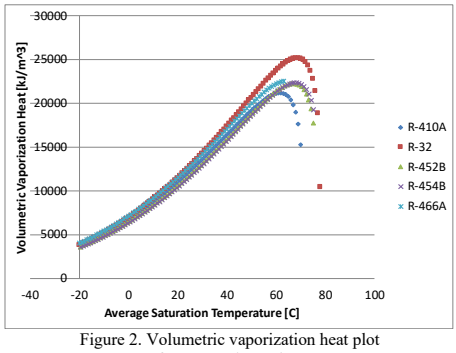

Figure 2. Volumetric vaporization heat plot of R-410A alternatives.

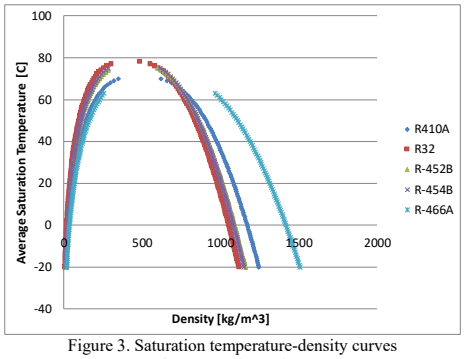

Figure 3. Saturation temperature-density curves of R-410A alternatives.

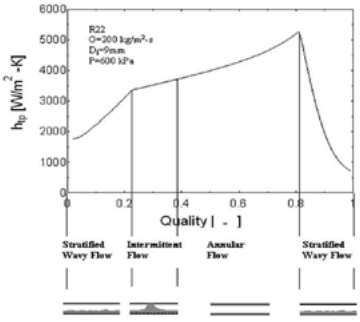

Figure 4: Local flow boiling coefficient predicted with the Thome (2002) [1] flow-pattern-dependent evaporation model.

Figure 3 shows curves of saturation temperature versus density of the R-410A alternatives. Most of the R-410A alternatives, except R-466A, have lower suction vapor density and lesser refrigerant mass flow rate if using a fixed compressor displacement volume.

At an average saturation temperature, a refrigerant with a lower volumetric vaporization heat results in smaller cooling capacity during a drop-in replacement. The saturation temperature is also impacted by the heat transfer performance and refrigerant pressure drop of the refrigerant. Lower saturation temperature leads to smaller cooling capacity if using the same compressor. And thus, whether an alternative low GWP refrigerant leads to higher or lower capacity depends on the trade-off between its volumetric vaporization heat and the resultant suction saturation temperature impacted by its heat transfer characteristics.

3. Model Description

A public-domain HVAC equipment modeling and design tool (HPDM, Shen 2016 [2]) was used to model a baseline heat pump. Some features of the HPDM, related to this study, are introduced below:

Compressor model:

AHRI 10-coefficient compressor maps (ANSI/AHRI 540-99, 2010 [3]) are used to calculate mass flow rate and power consumption, and enable calculation of the refrigerant-side vs. air-side energy balance from inlet to outlet by inputting a compressor shell loss ratio relative to the power input. It also considers the actual suction state to correct the map mass flow prediction.

We obtained the original compressor maps, developed for R-410A. For modeling the alternative refrigerants, it is assumed that the compressor would maintain the same volumetric and isentropic efficiencies at the same suction and discharge pressures. Thus, the efficiencies were reduced from the original R-410A map as a function of the suction and discharge pressures. The volumetric efficiency is defined in Equation 1, and isentropic efficiency is shown in Equation 2.

$$m_r = Volume_{displacement} \times Speed_{rotation} \times Density_{suction} \times \eta_{vol} \quad (1)$$

$$Power = m_r \times (H_{discharge,s} - H_{suction}) / \eta_{isentropic} \quad (2)$$

Where $\boldsymbol{m_r}$ is compressor mass flow rate; $\boldsymbol{Power}$ is compressor power; $\boldsymbol{\eta_{vol}}$ is compressor volumetric efficiency; $\boldsymbol{\eta_{isentropic}}$ is compressor isentropic efficiency; $\boldsymbol{H_{suction}}$ is compressor suction enthalpy; $\boldsymbol{H_{discharge,s}}$ is the enthalpy obtained at the compressor discharge pressure and suction entropy. The approach converting the compressor map of a baseline refrigerant to be used by its drop-in replacements has been extensively validated in Shen et al. (2018) [4].

Heat Exchanger Models:

Segment-to-segment fin-&-tube condenser: It uses a segment-to-segment modelling approach, which divides a single tube to numerous mini segments; each tube segment has individual air side and refrigerant side entering states and considers possible phase transition. An ε-NTU approach is used for heat transfer calculations within each segment. Air-side fin is simplified as an equivalent annular fin. Both refrigerant and air-side heat transfer and pressure drop are considered. The coil model can simulate arbitrary tube and fin geometries and circuitries, any refrigerant side entering and exit states, maldistribution, and accept two-dimensional air side temperature, humidity and velocity local inputs; the tube circuitry and 2-D boundary conditions are provided by an input file.

Segment-to-segment fin-&-tube evaporator: In addition to the functionalities of the segment-to-segment fin-tube condenser, the evaporator model is capable of simulating the dehumidification process. The method of Braun et al. (1989) [5] is used to simulate cases of water condensing on an evaporating coil, where the

driving potential for heat and mass transfer is the difference between enthalpies of the inlet air and saturated air at the refrigerant temperature. As noted, the segment-to-segment modelling approach can reveal the glide of a zeotropic refrigerant, since the temperature increment is accounted by each individual segment along the refrigerant flow path.

Through an extensive literature survey, we identified heat transfer and pressure drop correlations suitable for modeling and optimizing air conditioners and heat pumps, to assess various low GWP refrigerants. The correlations are listed in Table 2.

Table 2. Selected correlations for two-phase heat transfer and pressure drop

Application	Correlation
Fin-&-tube heat exchanger (FTC) -Evaporation heat transfer	Thome (2002) [1]
FTC-Condensation heat transfer	Cavallini et al. (2006) [6]
FTC-Evaporation pressure drop	Kedzierski and Choi (1999) [7]
FTC-Condensation pressure drop	Kedzierski and Choi (1999) [7]

The two-phase heat transfer correlations developed by Thome (2002) [1] and Cavallini (2006) [6] account for local flow patterns, considering refrigerant properties. The idea of the flow-pattern dependent evaporation model is to first estimate the wetted surface inside a horizontal smooth tube using a flow map prediction. The model covers stratified flow, stratified-wavy, annular-wavy, intermittent, annular flow, annular flow with partial dryout, and mist flow in evaporation. The general expression for local evaporating heat transfer coefficient is of the form,

$$h_{tp} = \frac{\theta_{dry} h_v + (2\pi - \theta_{dry}) h_{wet}}{2\pi} \tag{3}$$

$$h_{wet} = (h_{nb}^3 + h_{cb}^3)^{1/3} \tag{4}$$

In Equation 3, θ_{dry} is the dry angle corresponding to the dry circumference of the tube, which is determined from the flow pattern and void fraction. The void fraction model for this correlation is Rouhani (1970). h_{wet} is the heat transfer coefficient at the wet circumference of the tube, which is composed of a nucleate boiling term h_{nb} and a convective boiling term h_{cb}. h_v is the heat transfer coefficient at the dry circumference of the tube.

The local evaporation heat transfer coefficient calculated with the Thome (2002) [1] correlation is shown in Figure 4. The Thome (2002) correlation reasonably predicts degradation of heat transfer coefficient at high quality due to dry out of the liquid film, while most of the other correlations are not able to do this. This model can also reveal the effect of heat flux.

The condensation correlation of Cavallini (2006) [6] is given in Equation 5,

$$h_{tp} = \frac{\theta_{film} h_f + (2\pi - \theta_{film}) h_c}{2\pi} \tag{5}$$

θ_{film} is the falling film angle around the perimeter of the tube, which is dependent on the local flow pattern and void fraction. h_f is the Nusselt film condensing coefficient, and h_c is the convective condensation heat transfer coefficient. The Cavallini (2006) [6] condensation model also starts with the flow pattern prediction.

It is reported that azeotropic refrigerant mixtures have the same heat transfer performance as pure refrigerants. Thus, pure refrigerant correlations are able to work for an azeotropic refrigerant mixture such as R-410A. However, zeotropic refrigerant mixtures with large temperature glides, have different behaviors.

Heat transfer correlations developed for pure refrigerants must be corrected if they are to be used for zeotropic refrigerants. Stephan et al. (1992) proposed a correction method for condensation as well as evaporation. In this method, the mixture heat transfer coefficient h_m is defined as,

$$h_m = [1/h_f + (\delta Q_{SV} / \delta Q_T)/h_g]^{-1} \tag{6}$$

where h_f is the heat transfer coefficient computed from a pure refrigerant heat transfer model and h_g is the heat transfer coefficient of the vapor phase, which can be calculated with the Dittus-Boelter equation. $\delta Q_{SV} / \delta Q_T$ is the ratio between the sensible heat transfer and the total heat transfer. Bell and Ghaly (1973)

suggested that if the total isobaric temperature glide is around 7-8 °C, then the ratio could be approximated as,

$$(\delta Q_{SV} / \delta Q_T) \approx x Cp_g (\Delta T / \Delta h_m) \quad (7)$$

Where ΔT is the temperature glide, Δh_m is the enthalpy of latent heat of the mixture, x is the quality, and Cp_g is the vapor specific heat.

We adopted air side heat transfer correlations specific to individual fin types, respectively for dry and wet surface. Dittus-Boelter correlations was adopted to modelled single-phase refrigerant tube side heat transfer.

Expansion Devices:

The compressor suction superheat degree and condenser subcooling degree or system charge are explicitly specified. As such, the expansion device is not solved here – a simple assumption of constant enthalpy process is assumed.

Fans and Blowers:

The air flow rate and power consumption were direct inputs from the laboratory measurements for the model calibrations.

Refrigerant Lines:

Temperature changes and pressure drops of suction, discharge and liquid lines were specified using the measured data from the experiments.

Refrigerant Properties:

We programmed interface functions to call REFPROP 10.0 (Lemmon, 2018) [7] directly; our models accept all the refrigerant types in the REFPROP 10.0 database, and also we can simulate a new refrigerant by making the refrigerant definition file according to the REFPROP 10.0 format, or look-up tables.

4. Baseline Heat Pump and Rating Conditions

The DOE/ORNL heat pump design model (HPDM) was used for analytical evaluations for a baseline heat pump having a two-speed compressor. The two-state heat pump has the total cooling capacity of 5-ton/17.6 kW at 35°C ambient temperature/26.7°C indoor dry bulb temperature (DB) and 19.4°C indoor wet bulb temperature (WB). The high and low speeds of the scroll compressor provide 100%/67% capacity. The indoor and outdoor heat exchangers are described in Table 3. For the system modeling, the condenser exit subcooling degree was set at 10 R (5.6 K) for cooling mode and 20 R (11.2 K) for heating mode; the evaporator exit was assumed to have a constant superheat degree of 10 R (5.6 K).

Table 3: Parameters of Indoor and Outdoor Units

Parameters (heating mode)	Indoor Fin-&-Tube Coil	Outdoor Fin-&-Tube Coil
Face area, ft2 (m2)	3.30 (0.307)	22.3 (2.07)
Total Tube Number	84	64
Number of rows	3 (cross counter-flow)	2 (cross counter-flow)
Number of parallel circuits	9	6
Fin density, fins/ft (fins/m)	168 (551)	264 (866)
	Indoor Blower (High/Low[1])	Outdoor Fan
Flow Rate, cfm (m3/s)	1670/1380 (0.790/0.653)	3500 (1.652)
Power [W]	322/203	300

1. The indoor blower has two speed levels, corresponding to the compressor low/high speeds respectively.

Following the AHRI 210/240 standard [9] to rate a two-speed heat pump. In cooling mode, the heat pump should provide performance indices at 35°C, 27.8°C ambient temperature and indoor condition of 26.7°C DB/19.4°C WB. In heating mode, the heat pump should be rated at the indoor dry bulb temperature of 21.1°C. At the low speed, the ambient temperature should vary at 16.7°C DB/13.6°C WB, 8.3°C DB/ 6.1°C WB, 1.7°C DB / 0.6°C WB and -8.3°C DB / -9.4°C WB. The high speed should be rated at 8.3°C DB/ 6.1°C WB, 1.7°C DB / 0.6°C WB and -8.3°C DB / -9.4°C WB.

Since HPDM is a steady-state system model, it doesn't predict cyclic performance and frost/defrost penalty. We adopted a typical degradation coefficient of 0.1 for the high speed, and 0.15 for the low speed. AHRI 210/240 quantifies frosting/defrost loss at the outdoor condition of 1.7°C DB / 0.6°C WB. If no frost effect is

correlated by an analytical model, the standard recommends a 98% factor to scale the power consumption and a 91% factor to scale the heating capacity. AHRI 210/240 assumes no frost formation at the ambient temperature above 8.3°C DB/ 6.1°C WB and below -8.3°C DB / -9.4°C WB. At other ambient conditions, the performances are interpolated between 8.3°C DB/ 6.1°C WB, 1.7°C DB / 0.6°C WB; and interpolated between 1.7°C DB / 0.6°C WB and -8.3°C DB / -9.4°C WB. For the ambient conditions below -8.3°C DB / -9.4°C WB, the results are extrapolated based on the predicted results at 8.3°C DB/ 6.1°C WB and -8.3°C DB / -9.4°C WB.

5. Cooling Performance

Table 4 below presents predicted cooling performances of the heat pump using R-410A at the low (_L) and high speed (_H) levels, including cooling capacities [kW], cooling COPs [W/W], compressor discharge temperature [F] and compressor isentropic efficiency reduced from the compressor map in the form of Equation 2. The two-speed scroll compressor uses the full displacement volume at 100% capacity. At 67% capacity, only part of the scroll is utilized, which causes more loss factors. As a result, the compressor efficiency of the low speed is roughly 7% lower than the high speed.

Table 4: Predicted Cooling Performance Indices Using R-410A

Outdoor Condition	Capacity [kW]	COP [W/W]	Compressor Disc T [F]	Isentropic efficiency
35C_H	17.6	3.7	164.1	74%
27.7C_H	18.7	4.5	147.4	73%
35C_L	13.0	3.9	158.7	67%
27.7C_L	13.9	4.8	140.5	67%

Figure 5 show cooling capacity increments of the alterative refrigerant in comparison to R-410A, dropping into the same equipment. Corresponding to the vaporization plots in Figure 2, R-32 and R-466A result in 4% to 6% higher cooling capacities at all the conditions. On the other hand, R-452B and R-454B lead to approximately 2% smaller capacities. Figure 6 show increments in cooling COPs. With the same heat exchangers, larger capacity tends to cause higher condensing temperature and lower evaporating temperature, degrading the efficiency. Consequently, R-32 and R-466A have large capacities at the expense of reduced COPs. R-452B and R-454B result in higher COPs. Figure 7 presents compressor discharge temperatures. R-32 have significantly higher discharge temperatures, up to 30R. The other alternative refrigerants lead to minorly high temperatures, up to10R. At the low speed, the discharge temperatures are lower than those at the high speed, because the condensing temperature is reduced at the part-load operation. Figure 8 compares the seasonal cooling COPs, calculated from AHRI 210/240. They differ minorly, ranging from 4.45 to 4.58. R-454B results in the highest COP and R-466A results in the lowest COP.

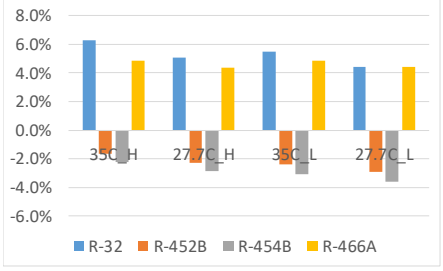

Figure 5. Capacity increments in cooling mode

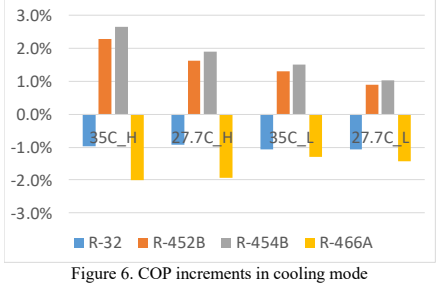

Figure 6. COP increments in cooling mode

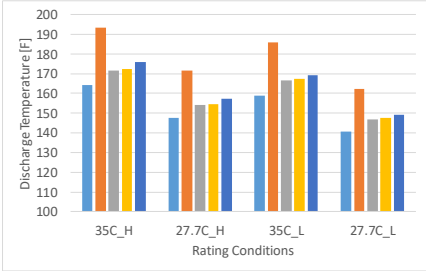

Figure 7. Compressor discharge temperatures in cooling mode

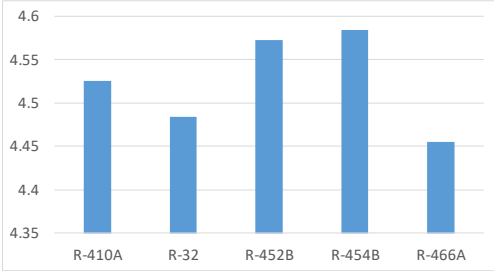

Figure 8. Seasonal cooling COPs

6. Heating Performance

Table 5: Predicted Heating Performance Using R-410A

Outdoor Condition	Capacity [kW]	COP [W/W]	Compressor Disc T [F]	Isentropic efficiency
8.3C_H	17.6	3.9	167.1	72%
1.7C_H	15.0	3.6	166.7	70%
"-8.3C"_H	11.4	3.0	172.8	64%
16.7C_L	15.8	4.5	165.7	66%
8.3C_L	12.8	3.9	165.7	63%
1.7C_L	10.8	3.4	170.1	59%
"-8.3C"_L	7.9	2.6	190.8	50%

Table 5 predicts heating performances using R-410A at the low (_L) and high speed (_H), including heating capacities [kW], heat pump heating COPs [W/W], compressor discharge temperatures [F] and the compressor isentropic efficiencies. Comparing the high speed with the low speed at low ambient temperatures, the efficiency degradation is more pronounced because the loss factors ascend with the compressor pressure ratio. At -8.3°C, the isentropic efficiency decreases from 64% to 50% when the pressure ratio increases from 3.4 to 4.2.

A typical heat pump sized to meet the building cooling load can't satisfy heating load at low ambient temperatures. Figure 9 compares the heat pump capacities as a function of the ambient temperature, versus the building load line of DHR_{min} defined in AHRI 210/240 in the ASHRAE climate zone IV. DHR_{min} indicates a well-insulated building. Even in the adequately insulated home, the heat pump total capacity still can't provide enough heating capacity. The high speed will be called at the ambient temperature below 25°F. Below 15°F, the high-speed operation can't meet the building heating load, and then, supplemental resistance heat will be used.

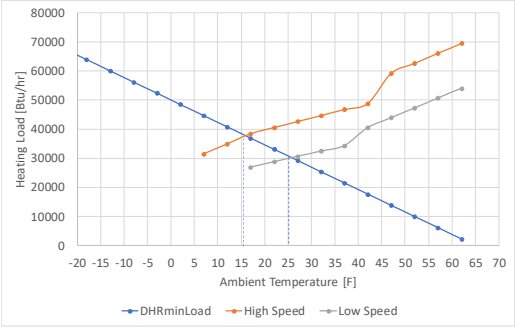

Figure 9: Heat Pump Capacities versus building load line

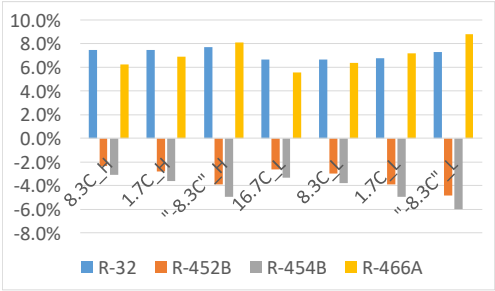

Figure 10. Capacity increments in heating mode

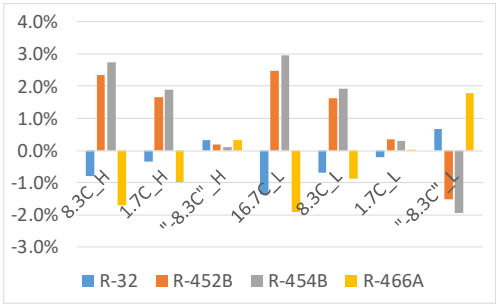

Figure 11. COP increments in heating mode

Figure 10 shows capacity increments of the alterative refrigerants versus R-410A in heating mode. R-32 and R-466A result in 6% to 8% higher heating capacities, which increase with decreasing the ambient temperature. On the other hand, R-452B and R-454B lead to approximately 2% to 6% smaller capacities, which decrease with the ambient temperature. Figure 11 shows increments in the heat pump heating COPs. R-32 and R-466A lead to 2% lower COPs due to the increased heating capacities. R-452B and R-454B lead to 2% higher COPs. Figure 12 presents compressor discharge temperatures. Because of the noticeably lower isentropic efficiency of the low speed at low ambient temperatures, more compressor power is converted to heat the refrigerant vapor than providing more useful pressure energy. Thus, the compressor discharge temperatures at low speed are higher than those at high speed. This is opposite to the trend, shown in Figure 7 regarding the cooling mode.

The discharge temperature increases with the pressure ratio, which tends to be higher in heating mode. Limit of discharge temperature is the major reason preventing heat pump operating below a certain ambient temperature. The higher discharge temperatures of the R-410A replacements would narrow the working envelope. The significantly higher discharge temperatures of R-32 (>210°F at -8.3°C) would require compressor lubricant change for the heat pump application. Figure 13 compares the seasonal heating COP, i.e. HSPF calculated by AHRI 210/240. Larger heating capacity causes degradation in heat pump COP, however, it decreases the supplemental resistance heat use at low ambient temperatures. As a result, the seasonal heating COPs are almost identical, regardless of the variations in heating capacity.

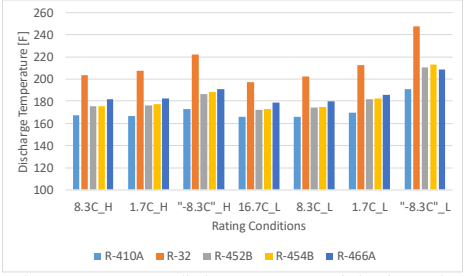

Figure 12. Compressor discharge temperatures in heating mode

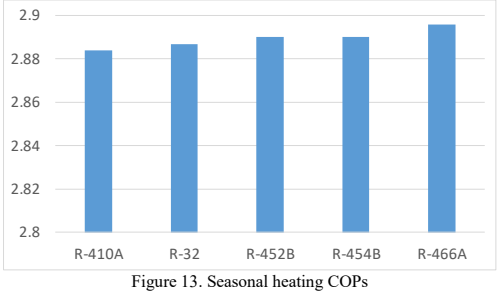

Figure 13. Seasonal heating COPs

7. Summary

This study starts with a hardware-based heat pump system simulation and design model, which adopted fundamental flow-pattern-dependent heat transfer correlations to represent variations in refrigerant properties. A method, to convert a baseline refrigerant compressor map used by alternative refrigerants in the similar pressure range, was developed and validated. Using the advanced analytical tool, we assessed lower GWP refrigerants to replace R-410A, in a drop-in application with respect to a two-speed heat pump. The alternatives include R-32, R-452B, R-454B and R-466A. The performance indices were predicted at the rating conditions of the AHRI 210/240 standard. Additionally, the seasonal cooling efficiency (SEER) and heating efficiency (HSPF) were compared.

In summary,

1) In cooling mode, R-32 and R-466A led to higher capacities, but slightly lower COPs than R-410A. R-452B and R-454B had very similar performance, having slightly lower capacities but higher COPs. R-454B resulted in the highest seasonal COP, and R-466A resulted in the lowest seasonal COP. In general, they differ minorly, ranging from 4.45 to 4.58.
2) In heating mode, R-32 and R-466A led to higher capacities, which degraded the heat pump heating COPs. R-452B and R-454B had slightly lower capacities but higher COPs. Larger heating capacity causes degradation in heat pump COP, but reducing the supplemental resistance heat use at low ambient temperatures. As a result, the seasonal heating COPs are almost identical among these refrigerants.
3) R-32 causes significantly higher discharge temperatures; R-466A, R-452B and R-454B results in moderately higher discharge temperatures. The higher discharge temperatures may narrow the operation envelope, particularly in heating mode. It is necessary to change the compressor lubricant for R-32, to tolerate the high discharge temperature during heating mode or cooling mode at elevated ambient temperature.

Acknowledgements

This research was supported by the DOE Office of Energy Efficiency and Renewable Energy, Building Technologies Office (BTO). The authors would like to acknowledge Mr. Antonio Bouza, Technology Manager – HVAC&R, Water Heating, and Appliance, DOE/BTO. This manuscript has been authored by UT-Battelle, LLC under Contract No. DE-AC05-00OR22725 with the U.S. Department of Energy. The United States Government retains and the publisher, by accepting the article for publication, acknowledges that the United States Government retains a non-exclusive, paid-up, irrevocable, world-wide license to publish or reproduce the published form of this manuscript, or allow others to do so, for United States Government purposes. The Department of Energy will provide public access to these results of federally sponsored research in accordance with the DOE Public Access Plan (http://energy.gov/downloads/doe-public-access-plan).

References

[1] Thome J.R. and Jean Ei Hajal, "Two-phase flow pattern map for evaporation in horizontal tubes: lastest version", 1st International Conference on Heat Transfer, Fluid mechanics, and Thermodynamics, 8-10 April 2002, Kruger Park, south Africa TJ2
[2] Shen, B. and Rice, K., 2016, DOE/ORNL Heat Pump Design Model, Web link: http://hpdmflex.ornl.gov/
[3] ANSI/AHRI Standard 540-99, 2010, “Positive Displacement Refrigerant Compressors and Compressor Units”, Air Conditioning and Refrigeration Institute, Arlington, VA.
[4] Bo Shen, Omar Abdelaziz, Som Shrestha, Ahmed Elatar, Model-based optimizations of packaged rooftop air conditioners using low global warming potential refrigerants, International Journal of Refrigeration, Volume 87, 2018, Pages 106-117, ISSN 0140-7007
[5] Braun. J.E., Klein. S.A, and Mitchell, J.W., 1989, “Effectiveness models for cooling towers and cooling coils”, ASHRAE Transactions, Vol. 95, Pt. 2, pp. 164-174.
[6] Cavallini, A, D.D. Col, L. Doretti, et al., Condensation in horizontal smooth tubes: a new heat transfer model for heat exchanger design, Heat Transfer Eng. 27 (8) (2006) 1–38.
[7] Lemmon E. W., Huber M. L., 2018 “NIST Reference Fluid Thermodynamic and Transport Properties Database (REFPROP): Version 10.0”, http://www.nist.gov/srd/upload/REFPROP10.pdf
[8] Kedzierski, M. A. and Choi J. Y., 1999, “A generalized pressure drop correlation for evaporation and condensation of alternative refrigerants in smooth and micro-fin tubes”, NISTIR 6333.
[9] AHRI 2008. ANSI/AHRI Standard 210/240-2008, “Performance Rating of Unitary Air-Conditioning and Air Source Heat Pump Equipment,” Air-Conditioning, Heating, and Refrigeration Institute, Arlington, VA, USA.